ACS OMEGA

Open Access

http://pubs.acs.org/journal/acsodf

Article

Impact of Porous β-Tricalcium Phosphate Microspheres on Curcumin-Loaded Brushite Bone Cement for Bone Regeneration

Garima Tripathi, Myeongki Park, Seong-su Park, Hai-Doo Kim, Byoung-Ryol Lee, and Byong-Taek Lee*

Cite This: *ACS Omega* 2025, 10, 14961−14971

Read Online

ACCESS | Metrics & More | Article Recommendations | Supporting Information

ABSTRACT: The current study aimed to create a modified injectable bone substitute (IBS) with improved osteogenic characteristics. To enhance the cement injectability and release properties of curcumin in vitro, we incorporated curcumin into β-tricalcium phosphate (β-TCP) to create the composite supplemented with sintered porous β-TCP microspheres, which maintained good injectability with an initial setting time of 5.0 ± 1.3 min and a mechanical strength of 20.67 ± 1.3 MPa for bone cements. The differentiation potential of preosteoblast (MC3T3-E1) to osteoblasts was significantly boosted by incorporating curcumin, which triggered Col I, upregulated OPN expression, and boosted alkaline phosphatase activity. Bone regeneration was hastened after the in vivo implantation of curcumin-modified brushite (BR4P2C) cement into the implanted femoral defects, and the rate of cement disintegration was accelerated. As a result, the translational application of modified BR4P2C in preliminary research has the potential to serve as an IBS with curcumin, which has an exceptional ability to repair bone lesions.

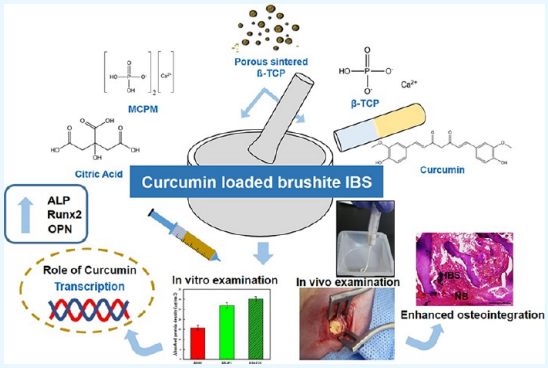

1. INTRODUCTION

Calcium phosphate cements (CPCs) have been utilized successfully in the repair of critical-size bone lesions due to their excellent bone-forming capabilities.[1] Brushite is one of the members of the CPC group, which has drawn the interest of academics because of its promising degradation behavior and bone-remodeling capability under in vivo conditions.[2] Also, the easy injectability and suitable setting window time of brushite provide ease of handling to the clinical practitioner for minimally invasive surgery.[3] Various compositions have been used to make the brushite-forming CPCs a suitable injectable bone substitute (IBS) system. However, research is still going on to find suitable compositions according to the patient-specific bone defects depending upon their age group.

An exciting research topic in recent years has been the application of microspheres in bone tissue engineering by utilizing their large specific surface area, which facilitates cellular growth and proliferation.[4] Incorporating porous spheres in the bulk scaffold is helpful for bioactive molecule loading and their release profile. Spray-drying is a unique process for preparing monodispersed spherical powders with a controlled microstructure, pore size, pore volume, and good flowability.[5] The controlled microstructure provides adequate control of the degradation profile and thereby controls the release of the bioactive molecules that regulate bioactivity. Moreover, this process is effective for developing porous-sphere-based injectable brushite systems where these spheres can be uniformly distributed.[6] On the other hand, the faster degradation rate of the porous spheres generates a porous structure in the cement, which ensures the supply of blood and nutrients for a suitable microenvironment for new bone tissue growth. The uniform distribution of the spheres throughout the IBS is an issue considering the mechanical strength for which a suitable composition needs to be realized.

Curcumin is a natural substance, commonly called curcuminoids, obtained from the root of the turmeric herb (Curcuma longa).[7] It has been utilized widely in Indian Ayurvedic treatment for many years and is also frequently found in regular dietary intake. In today's modern scientific world, curcumin has been found effective against cancer, inflammation, insulin resistance, obesity, and diabetes mellitus.[8−11] According to a previous report, the natural antioxidant curcumin has a synergistic impact when used in combination with chemotherapeutic drugs to treat cancers of the bone, ovary, and lung.[12] Preclinical studies have shown that curcumin regulates the nuclear factor-$\kappa\beta$ ligand and vascular endothelial growth factor, which are involved in bone remodeling.[13]

The curcumin-loaded system is designed to interact with bone tissue through various mechanisms. Curcumin, known for

Received: November 13, 2024
Revised: March 25, 2025
Accepted: April 2, 2025
Published: April 11, 2025

its anti-inflammatory and osteogenic properties, promotes osteoblast differentiation and bone matrix mineralization, which are crucial for bone formation and healing. It also modulates the activity of osteoclasts, potentially reducing excessive bone resorption during the healing process. The slow degradation rate of the tricalcium phosphate (TCP) microspheres ensures the sustained release of curcumin and other bioactive molecules, which further enhances bone regeneration. Additionally, the microporous structure of the microspheres facilitates cell infiltration and provides a scaffold for new bone growth.[14] These combined effects contribute to the potential of the material to support bone repair and regeneration, making it a promising candidate for bone tissue engineering.

Moreover, curcumin can upregulate cell-proliferation-related gene expression and enhance osteoblast viability, indicating its great potential in bone tissue-engineering applications.[13] Therefore, to determine the osteogenic activity, curcumin was incorporated in ceramics scaffolds such as β-TCP and HA, which significantly enhanced osteoblast cell proliferation and reduced osteosarcoma activity.[15−17] Bose et al. prepared a 3D-printed β-TCP scaffold incorporated with curcumin, which was implanted in the distal femur bone of a rat, and found an increase of ∼15% bone formation after 6 weeks.[15]

A detailed examination of the bone regeneration potential of the curcumin-loaded brushite-based IBS is yet to be conducted. A systematic in vitro study on cell proliferation, differentiation, and in-depth analysis of in vivo bone remodeling capability is necessary to evaluate the pharmacological effects of the curcumin-loaded brushite system in bone tissue engineering. Apparently, we prepared curcumin-loaded injectable brushite using β-TCP powders for bone grafting. After that, further modification and substitution of β-TCP powders with the sintered β-TCP microspheres were carried out to improve the capability of brushite for easy application at bone defects.

Consequently, the current investigation aimed to assess the bone-remodeling potential of the injectable brushite by mixing different fractions of β-TCP powder and microspheres after incorporating curcumin. We determined the microstructure, physicomechanical properties, cytocompatibility, and osteogenic differentiation of the samples. Micro-CT and histological analyses were carried out to examine the bone regeneration capacity of the samples after injection at the defect sites in rabbit femur bone after 1 and 2 months.

2. MATERIALS AND METHODS

2.1. Sample Preparation. The cements were prepared by a physical cement-mixing procedure. Compositions of the materials are presented in Table 1. For curcumin loading, the stock solution was prepared and loaded in the powder for further processing to achieve homogeneous distribution throughout the in vitro and in vivo examinations. β-TCP porous microspheres were prepared using the aqueous slurry in the presence of a binder and PMMA microspheres for pore generation, followed by the spray-drying method. Complete drying of the spray-dried powder was followed by calcination and sintering to obtain porous microspheres (Figure S1). According to the ISO 9917 standard, the setting time for the prepared cement was chosen. Following an accepted protocol, the Gilmore needle test was performed to determine the initial and final setting times of the samples.

Table 1. Sample Names and Their Compositions

sample name	(A) β-TCP powder (wt %)	(B) β-TCP microsphere (wt %)	(C) MCPM (wt %)	(D) citrate (vol %)	(E) curcumin (μm)
BR60	6	0	4	0.5	10
BR5P1	5	1	4	0.5	10
BR4P2	4	2	4	0.5	10
BR3P3	3	3	4	0.5	10

2.2. Physicomechanical Analysis. Powder X-ray diffraction (XRD) analysis in the range of 2θ = 10°−50°, with a 2θ angle rate of 2°/min (D/MAX-250, Rigaku, Tokyo, Japan), was performed for phase analysis. Functional group analysis of the samples was conducted by Fourier transform infrared (FTIR) spectroscopy (C1000 Thermal Cycler) throughout a 4000−600 cm^{-1} wavelength range. The microstructure of the sample was examined by scanning electron microscopy (SEM, JSM-6701F, Japan). Before testing, the samples were platinum-sputter-coated (Cressington Scientific Instruments, U.K.). The prepared samples were mechanically compressed using universal testing equipment to test their strength. The test crosshead speed was 0.5 mm/min. The compression test specimen measured 6 mm × 12 mm.

2.3. In Vitro Degradation and Change in pH. Samples were submerged in phosphate-buffered saline to measure in vitro deterioration. Samples were shaken at 37 °C for 1, 2, and 3 weeks after immersion in PBS. Every 3 days, more solution was added. Samples were rinsed with deionized water at intervals. Following drying, the weights of the samples were determined to assess the dissolution rate using the formula given below:

$$\text{Degradation rate (\%)} = \frac{w_1 - w_2}{w_1} \times 100 \quad (1)$$

where w_1 is the initial weight and w_2 is the final weight.

The samples were immersed in osteoblast (7.4)- and osteoclast (5.2)-favorable pH solutions and shaken at 37 °C for pH measurement. The immersion media was not renewed during the trial. A pH meter (Thermo Scientific, Korea) monitored the pH of the immersion media after different time intervals for all of the samples.

After completion of the degradation study, the phase transformation was characterized by XRD and FTIR spectroscopy.

2.4. In Vitro Curcumin Release Behavior. It was noted that curcumin-loaded samples released curcumin in PBS for 35 days at 37 °C (pH 7.4). Targeted samples were placed in 1 mL of PBS in a 24-well plate. At 1, 2, 3, 4, and 5 h and 1, 2, 3, 4, 5, 6, 7, 8, 12, 14, and 15 days, PBS taken from wells was analyzed using a Biodrop#1005363 Spectrophotomer (Denville Scientific Inc., USA). Curcumin levels were calculated using a standard calibration curve.

2.5. In Vitro Biocompatibility Evaluation. Mouse-derived preosteoblast MC3T3-E1 cells were grown in a cell culture medium. The cells were incubated at standard cell culture conditions. The culture media were updated every 2−3 days. The samples were seeded at 1 × 10^5 cells/ml with 5% trypsin-EDTA to separate over 80% of confluent cells.

2.5.1. Cell Proliferation and Cell−Material Interaction. Cell proliferation in the samples was determined using EZ-Cytox (DoGenBio Co., Korea) after culturing for 1, 3, and 7 days with different doses of curcumin for optimization. Hence, EZ-Cytox solution (1:10) was added to each sample and kept

https://doi.org/10.1021/acsomega.4c10336
ACS Omega 2025, 10, 14961−14971

Scheme 1. Hypothetical Illustration of the Preparation of the Sample and Its Role in Bone Formation

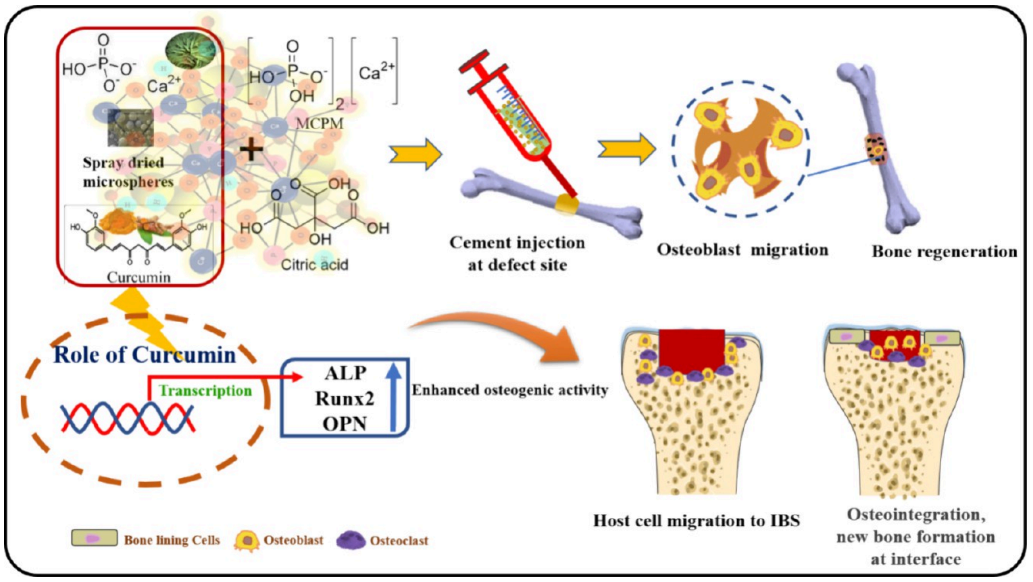

for 2 h in the incubator. After that, 100 μL of the supernatant liquid was aliquoted into a 96-well plate, and the absorbance was measured at 540 nm using a multimode plate reader (BioTek, USA).

Cell attachment on the sample surface was visualized to assess the cell−material interaction after different periods. The adhered cells on the sample surface after 5 days were determined using a scanning electron microscope (JSM-6701F, Japan). Before that, samples were covered with 4% PFA for 30 min for fixation of the cells. Then, a series of alcohol dilutions (50, 60, 80, 90, 95, and 100%) was used for the dehydration of the samples for 10 min in a duplicate manner. Finally, hexamethyldisilazane was used to dehydrate the fixed cells on the samples. Confocal microscopy (FV10i-W, Olympus, USA) was performed to monitor cell proliferation and spreading on materials after 1 and 7 days of incubation using our lab-established protocol.

2.5.2. In Vitro Mineralization. A test for in vitro mineralization was carried out in accordance with the method given in our previously published article.[18]

2.6. In Vivo Implantation and Post-Implantation Analysis. JSBIO (Korea) provided male New Zealand White Rabbits (12 weeks old). All procedures were carried out in accordance with the guidelines established by our Institutional Animal Care and Use Committee (Soon-chunhyang University, South Korea). Isoflurane (Piramal, India) inhalational anesthesia was used for all surgical procedures. The rabbits were assigned to groups at random for the implantation. The surgical site was sterilized with 70% ethanol and povidone-iodine, and an incision was made above the distal femoral head. The femur was then drilled with a trephine drill to generate a 6 × 5 mm defect while continuously rinsing with saline. The implant material was put into the faulty site with a 3 mL syringe. The incision region was sutured after implantation, and the animals were given antibiotics (Baytril, Bayer, Korea) and painkillers (Maritrol, JEILPHARM, Korea). Animals were sacrificed 1 and 2 months after implantation, and the implanted site was removed. All actions complied with the guidelines established by our Institutional Animal Care and Use Committee (Approval number: SCH 22-0072).

2.6.1. Micro-CT Analysis. Using μ-CT, bone development was investigated on the excised rabbit femur at 1 and 2 months after the implant had been placed. The examinations were conducted utilizing a Skyscan 1172 micro-CT scanner with a 1.5-megapixel camera (each pixel size was 8.81 μm) and software version 1.5. Images were acquired using a 70 kV source voltage, 120 μA current, 13.28 μm pixel size, 360° rotations, 7° step, and flat-field correction. Nrecon 1.6.9.8 batch reconstruction software was used to manage all scanned data. The data sets were 2000 × 1336-pixel bitmap images. Data viewer software 1.5.1 rotated and reoriented rebuilt data. Two ROIs were chosen for each bone micro-CT scan, and the % BV/TV was calculated.

2.6.2. Histological Analysis. The harvested bones were serially immersed in alcohol (70−100%) for dehydration after being decalcified with 5.0% nitric acid. Dehydrated samples were processed following xylene immersion, paraffin intrusion, and eventually embedding into paraffin blocks. Using a microtome (RM2255, Thermo Scientific, US), tissue sections (5 μm) were cut from the paraffin blocks and put on glass slides. The activity at the cellular level was examined by staining the slides with hematoxylin and eosin (H&E). Masson's trichrome (MT) was used to make the connective tissues visible at the surgical site. Using an attached DP72 camera and CellSens software, an Olympus BX53 research microscope was used to obtain images of the stained slides for examination.

2.7. Statistical Analysis. The mean standard deviation (SD) is presented for all experimental data. For comparison of data between the two groups, the Student *t*-test was used. ANOVA (one-/two-way, wherever applicable) with Tukey's multiple comparison test was used to examine data from different groups. For statistical analysis, GraphPad Prism 5.0 was utilized. The levels of significance were p 0.001***, p 0.01**, and p 0.05*.

https://doi.org/10.1021/acsomega.4c10336
ACS Omega 2025, 10, 14961−14971

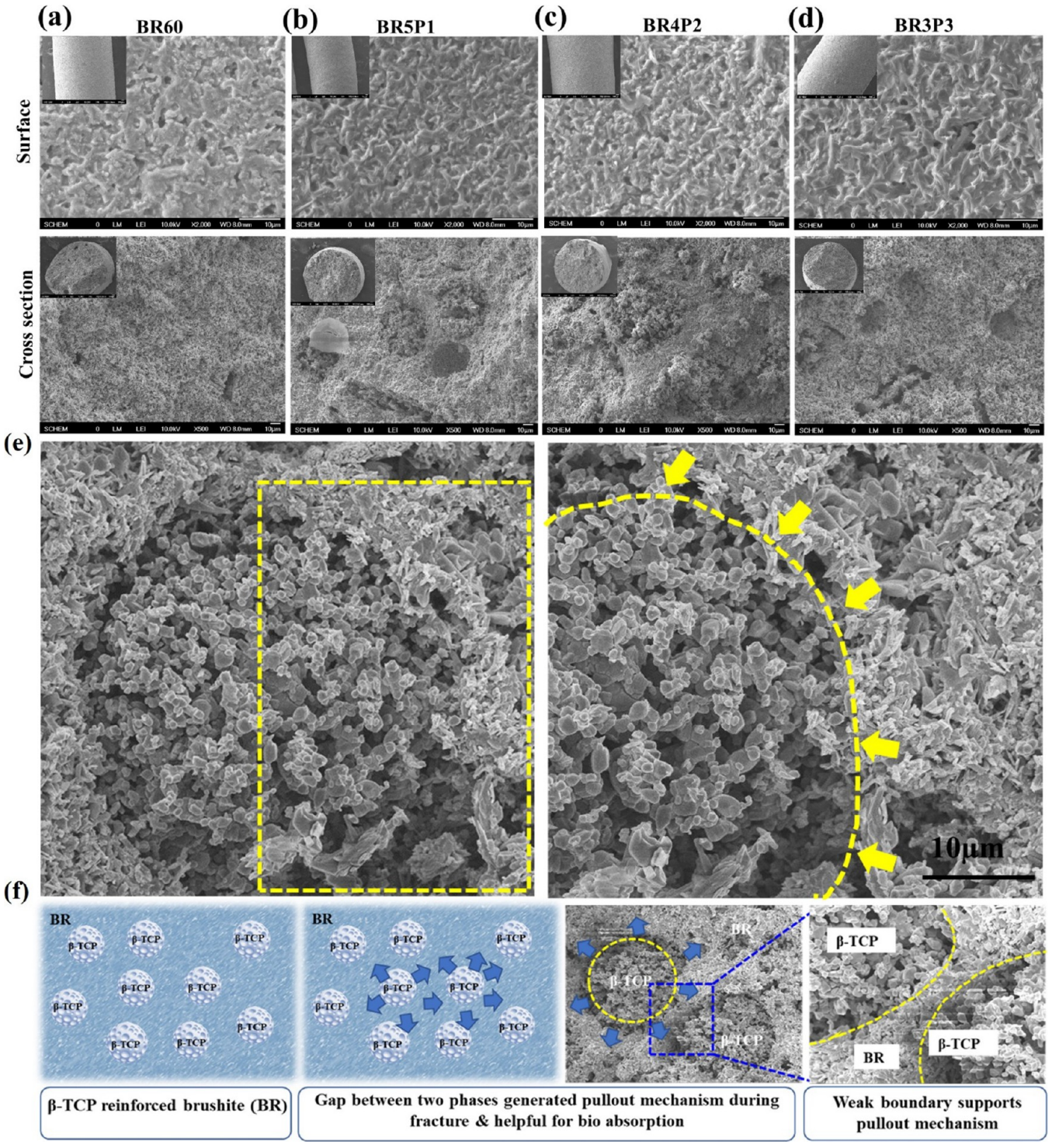

Figure 1. (a–d) Microstructures of the surface and cross section of the prepared bone substitute with varying concentrations of β-TCP. (e) Microstructure of the surface and cross section of BR4P2. (f) Illustration of the pull-out mechanism to support bio-absorption.

3. RESULTS AND DISCUSSION

3.1. Phase, Morphology, and Physicomechanical Properties. IBSs have gained popularity due to their characteristics, such as little invasiveness, security, and healing ability. As a result, we created a modified injectable bone cement that could prevent fractures or meet the need for repair in the early stages of osteoporosis. Scheme 1 summarizes the working hypothesis for this study, including sample preparation and the role in in vivo bone remodeling. The present study reinforced the brushite system with sintered porous β-TCP spheres and modified it with curcumin for enhanced osteoconductive and osteoinductivity. Curcumin may promote bone formation and regeneration by reducing H_2O_2-stimulated osteoblast apoptosis, improving mitochondrial function, and restoring high glucose-impaired osteogenic differentiation of osteoblasts and BMSCs.[19,20] Figure 1 displays the microstructure of the surface and cross sections of the prepared samples. The details of sample composition are provided in

https://doi.org/10.1021/acsomega.4c10336
ACS Omega 2025, 10, 14961−14971

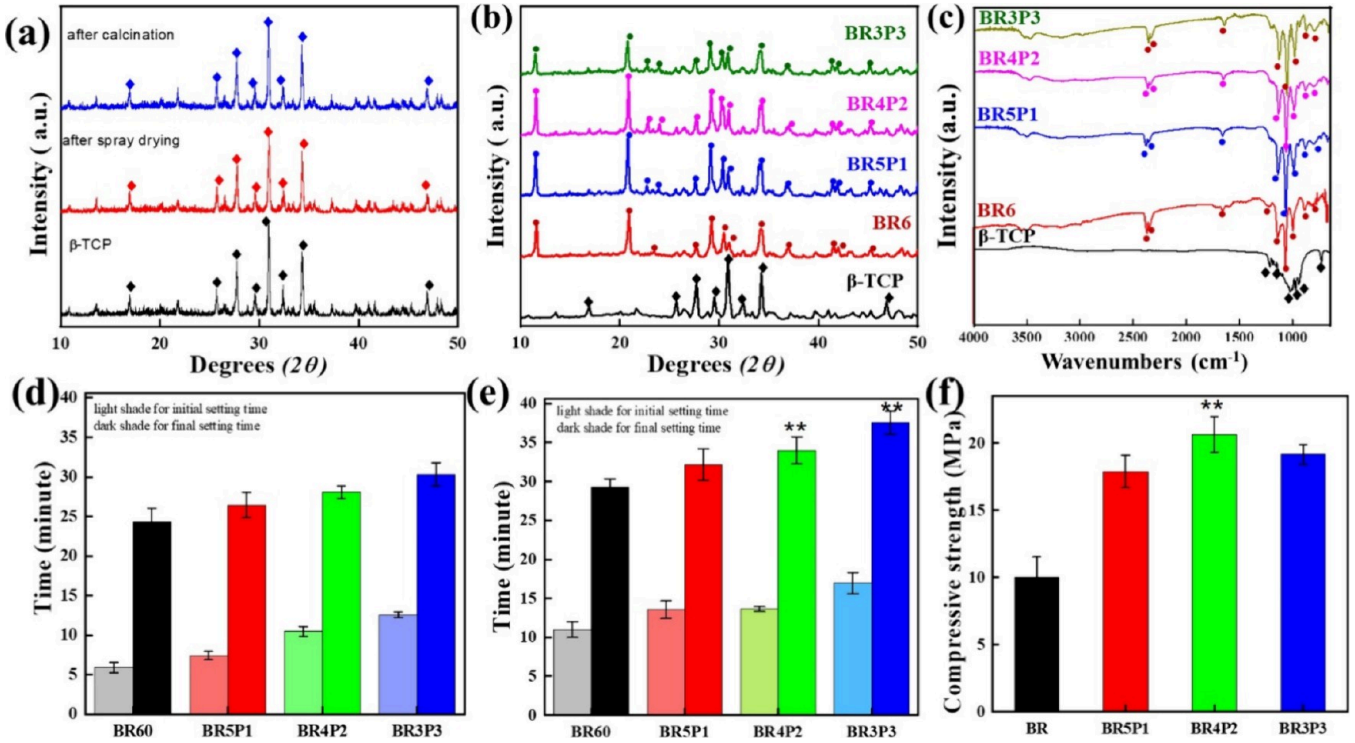

Figure 2. (a) In front of XRD patterns of the precursor as-synthesized β-TCP powder and porous β-TCP granules. (b) XRD traces of the prepared bone cement with varying porous sphere contents. (c) FTIR analysis of the prepared bone cement with varying porous sphere contents. Setting times in the (d) dry state and (e) wet environment (normal saline). (f) Compressive strength of prepared samples (under 1 Ton load).

Table 1. Common brushite crystal appearance was observed in a set of samples at the surface, but cross-sectional images evidenced the incorporation of sintered β-TCP reinforcement into the main matrix. High-magnification cross-sectional images of the BR4P2 sample are shown in Figure 1e. The area marked by the yellow dotted line depicts the appearance of two different microstructures. Reinforcement of β-TCP created a circular crater-like structure after the pull-out mechanism during the mechanical test, as shown in the cross-sectional image in Figure 1f. The overall pull mechanism of the gap in the grain boundary, which is further helpful for biosorption, is depicted in Figure 1f. Figure 2a confirms the purity of spheres of β-TCP after the sintering process. This β-TCP was further reinforced into the cement system. Figure 2b,c displays the XRD pattern and FTIR spectra for the difference compositions prepared with varying amounts of β-TCP reinforcement into the main matrix. The XRD spectra in Figure 2b show that the products were primarily brushite calcium phosphate, as indicated by XRD peaks at 2θ values of 11.9, 21.1, 29.5, 30.7, and 34.7. The only difference was the decrease in the crystallinity of the peaks on increasing the β-TCP portion. Also, it was noticed that due to the broadening, the peak at 30.7 of brushite overlapped with the most intense peak of β-TCP. Apart from these observations, no foreign phase was identified by either XRD or FTIR spectroscopy. The existence of the PO_4^{3-} groups concerning "β-TCP" is a typical peak. Figure 2c represents the FTIR spectra of all of the prepared samples. The PO_4^{3} groups of β-TCP were responsible for the bands at 1120, 1100, 1006, and 945 cm^{-1}. At 1640, hydroxyl groups were also observed (poor intensity). As previously mentioned, we verified the FTIR spectra of all of the sample preparations after establishing β-TCP conversion to brushite. The peak at 1649.19 cm^{-1} was related with H−O−H bending vibrations, whereas stretching vibrations connected with P═O were seen at 1215.19, 1126.47, and 1088.81 cm^{-1}. Weak absorptions at 1766.85 cm^{-1} were associated with HPO_4^{2-}.[21] P−O−P asymmetric stretching vibrations at 987.59, 862.21, and 808.20 cm^{-1} were discovered. The (H−O−) P═O bond in acid phosphate was attributed to two bands at 580.59 and 520.80 cm^{-1}.[22] Brushite crystal formation was confirmed by FTIR spectroscopy in the presence of P═O, O−H, and water of crystallization. After the setting reaction, all sample sets displayed XRD and FTIR peaks that were remarkably similar, and the main product was identified as brushite. In short, no foreign phase was found throughout the setting reaction, indicating the absence of any adverse reactions.

A short setting time limits the operative term for predicted CPCs, made by mixing powder and liquid in a specified ratio. If this connection is not made correctly, the cement may become unusable before implantation. The addition of β-TCP to the primary matrix gradually lengthened the hardening/setting time, as shown in Figure 2d,e. Initial and final setup times were carefully noted by utilizing $n = 6$ samples examined for all examined groups. The setting time was observed in both dry and wet environments, and in both conditions, the setting time was increased on increasing the content of β-TCP. Set IBS systems were shown to provide adequate compressive strength for fracture stabilization. Intriguingly, when β-TCP was introduced into the brushite matrix, a 2.3 times increase in the compressive strength was observed. A compressive strength of (9.89 ± 2.25) MPa was detected in BR60, while BR4P2 exhibited the highest strength of 22.01 MPa, as shown in Figure 2f. The trabecular bone has 4−12 MPa compressive strength and 50−800 MPa elastic modulus, while the human cortex shows corresponding values of 100−130 MPa and

https://doi.org/10.1021/acsomega.4c10336
ACS Omega 2025, 10, 14961−14971

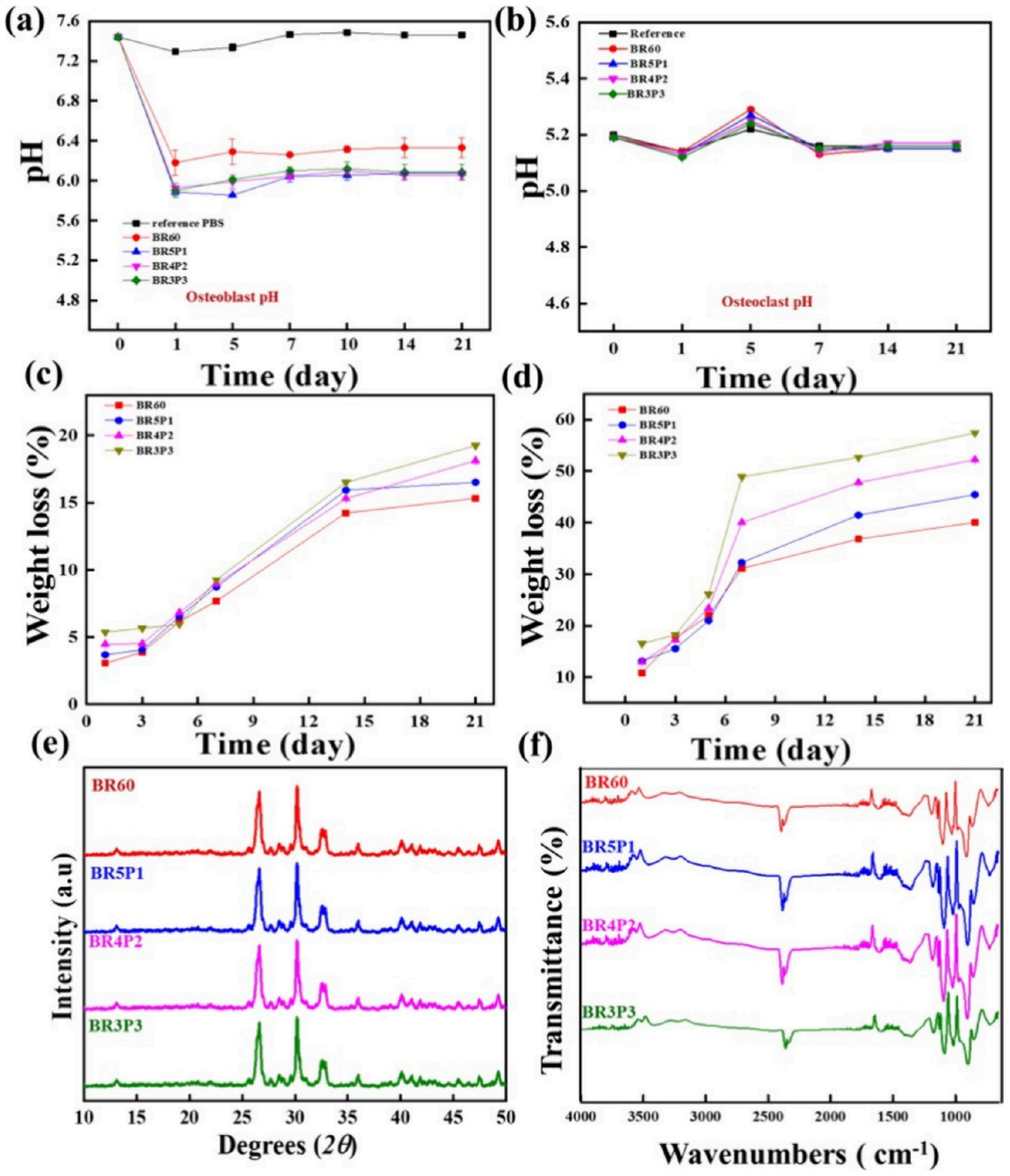

Figure 3. Change in pH after immersing samples in (a) osteoblast-favorable pH solution and (b) osteoclast-favorable pH solution. Changes in weight after immersing samples in (c) osteoblast-favorable pH solution and (d) osteoclast-favorable pH solution. (e) Post-degradation XRD and (f) post-degradation FTIR for confirming phase transformation in osteoblast-favorable pH solution.

17.9−18.2 GPa, respectively.[23] The clinical procedure is substantially impacted by the setting period. The surgical procedure was extended by the slow setting period of the cement.

3.2. In Vitro Degradation Cytocompatibility, Differentiation, and Curcumin Release Studies. Figure 3a−d summarizes the in vitro weight loss study and changes in pH for osteoblast- and osteoclast-favorable conditions that were carefully studied across multiple time frames to identify any unforeseen changes. Throughout the experiment, no unusual results were found. After 21 days of incubation, weight loss and an evident pH change in PBS were observed. After 21 days, a weight loss of ∼20% for osteoblasts with a favorable pH and ∼58% for osteoclasts with a favorable pH were noted. Figure 3e,f shows the post-degradation XRD and FTIR results, confirming the transition of brushite into other phases. XRD and FTIR data showed that brushite transformed into monetite after 24 h in PBS. It is possible that DCPD was formed as an intermediate in the premixed calcium phosphate systems because of the absence of sufficient water to generate DCPD. When DCPD decays into DCPA, water is released to endure the process. The DCPA XRD peaks were visible at 26.56°, 28.50°, and 30.16°.

Different doses were loaded on the optimized sample, i.e., BR4P2, to optimize the suitable curcumin concentration. After reproducing a similar trend, a 10 μM concentration was found to be ideal for cell survival in vitro. Figure 4 shows the cumulative release profile of curcumin. Until 45 days, there was

https://doi.org/10.1021/acsomega.4c10336
ACS Omega 2025, 10, 14961−14971

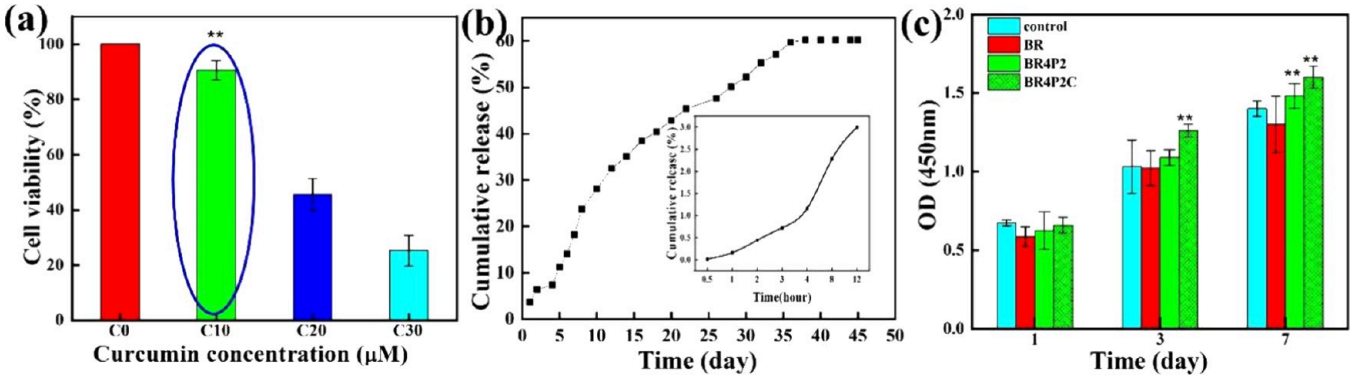

Figure 4. (a) Cytoxicity evaluation for various curcumin concentrations. (b) % Cumulative release until 45 days. (c) Cell viability on days 1, 3, and 7 on the prepared samples with 10 μM concentration. The levels of significance were p 0.001***, p 0.01**, and p 0.05*.

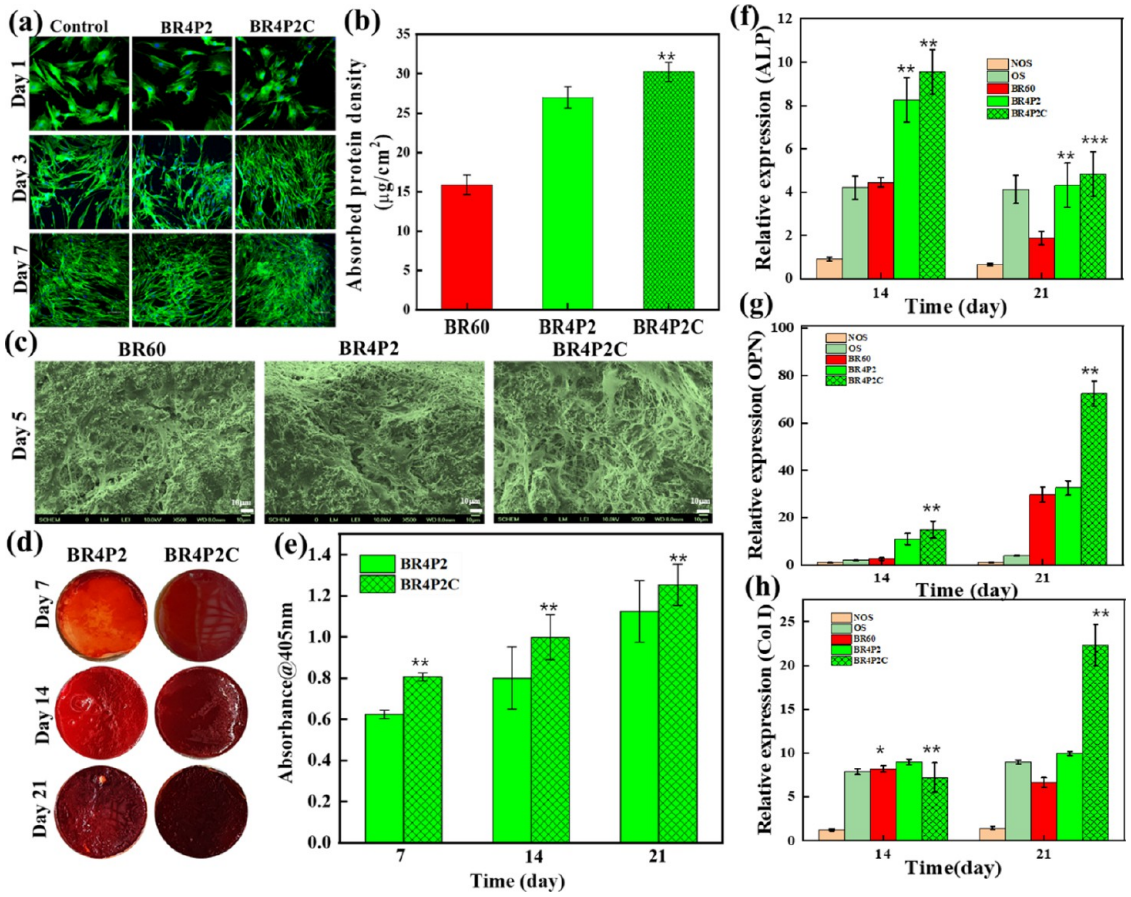

Figure 5. (a) Cell proliferation behavior. (b) Protein absorption behavior. (c) Cell adhesion behavior on the prepared samples at day 5. (d) Qualitative and (e) quantitative mineralization using MC3T3-E1 cells. (f) ALP gene expression, (g) osteopontin gene expression, and (h) collagen type I gene expression over 21 days of curcumin-loaded brushite with monolayer cultures seeded with MC3T3-E1 cells in osteogenic conditioned medium.

approximately ∼68% release, which is acceptable owing to the aquaphobic behavior of curcumin. A further optimized concentration was loaded onto BR4P2 and investigated for the cell viability test. Figure 6c demonstrate that curcumin improved O.D. levels over time.

Confocal microscopy images of the seeded cells after 1, 3, and 7 days of incubation (Figure 5a) were used to demonstrate the cell morphology and proliferation more clearly. To gain a better understanding, we analyzed the SEM images to confirm cell adhesion onto the surface of the prepared samples. Direct cell attachment behavior on the ready-made sample surfaces is depicted in the SEM micrographs in Figure 5c. The information in Figure 5a shows that with the progression of time, there was an increase in the number of seeded cells, and the cells of the samples became more interconnected. More cytoplasmic extension could be seen across the entire surface, and cells were flattened. Surprisingly, we discovered viable cells on the surface, and cell multiplication was pretty remarkable after brushite was added with curcumin.

Overall, the modified BR4P2C exhibited the best performance among all of the evaluated samples. To obtain evidence that the improved biocompatibility is accurate, we carried out

https://doi.org/10.1021/acsomega.4c10336
ACS Omega 2025, 10, 14961−14971

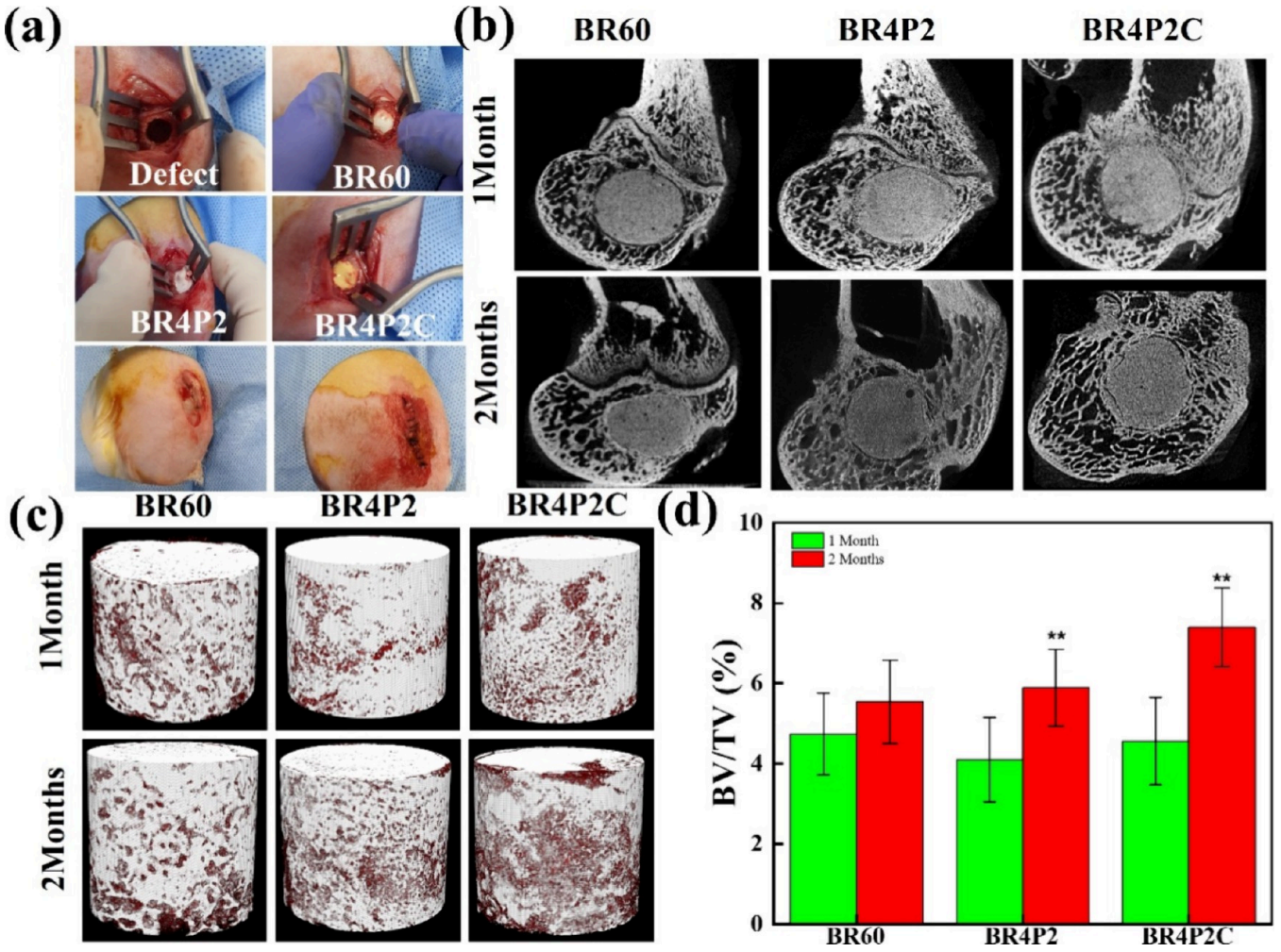

Figure 6. (a) Images obtained during in vivo implantation. (b) 2D images of post-implanted samples. (c) 3D images for the extracted samples. (d) BV/TV % for the extracted samples at 1 and 2 months post-implantation.

additional in vitro research on the protein absorption behavior of the produced samples (shown in Figure 5b) and the mineralization behavior (shown in Figure 7d,e). The addition of curcumin to the brushite matrix had a slight effect on the amount of protein absorbed. Concerning mineralization, the cytoplasmic layer was produced after 7, 14, and 21 days of incubation of MC3T3-E1 cells on the sample in an osteogenic growth medium. A meaningful change was observed when compared with the unmodified and curcumin-loaded samples; however, there was no significant difference after day 21. Yet, it was interesting to note an increase in mineralization after day 21. Increased ECM mineralization with the addition of curcumin is proof of its bone regenerative capability. Calcium deposition followed the aforementioned phenomenological pattern, which was validated by qualitative and quantitative ECM mineralization analyses. The mean staining area was calculated using ARS micrographs as a data source.

Real-time quantitative PCR (RT-qPCR) was utilized to analyze the effects of curcumin on the expression levels of ALP, OPN, and Col-1, as summarized in Figure 5f–h. During the early stages of development, Runx2 also promoted the expression of Col-1 and other osteogenic genes and OPN with the development progression. Col-1 is an essential extracellular protein in bone and one of the vital biological components of the bone matrix. The bone matrix contains a significant amount of Col-1, an organic component. Osteoblasts release a phosphorylated glycoprotein called OPN, which has been shown to stimulate bone biomineralization and remodeling.

Furthermore, it has been suggested that the particular interaction between OPN and Col-1 might organically restrict OPN, hence affecting osteoblast adherence, differentiation, and function.[24] Because ALP is a well-known early marker, BR4P2C expression was shown to be highest at day 14, with a gradual decrease through day 21. The expressions of OPN and Col-1 were drastically boosted after introducing curcumin. Compared to BR4P2, the BR4P2C group had significantly greater OPN and Col-1 gene expressions ($p < 0.05$). The findings revealed that the osteogenic effect of curcumin was observed only in the first stage of osteogenesis.[25] Curcumin upregulated the expression of Col-1 in precursor osteoblasts, although the regulation mechanism for OPN is distinct from that of Col-1. The data presented here show that curcumin induced osteoblastic differentiation of preosteoblasts MC3T3-E1 cells. Hence, it is proposed that curcumin may help restore osteogenic differentiation in precursor osteoblasts.

3.3. In Vivo Implantation, Micro-CT, and Post-Implantation Histological Evaluations. Figure 6a represents the digital images obtained during in vivo implantation. The micro-CT scans performed on the bone samples revealed

https://doi.org/10.1021/acsomega.4c10336
ACS Omega 2025, 10, 14961−14971

that the removed tissue was similar to its host bone. Figure 6b displays the 2D images of the rabbit femur when the implant was placed. Higher cement deterioration can be seen in Figure 6c at the bone−implant interface 1 month after BR4P2 and BR4P2C implantation, and this trend was accelerated by 2 months, as evident in the 3D images. New bone formation was substantially higher with BR4P2C implants than with BR60 and BR4P2 implants ($p < 0.05$), quantified by comparing bone volume fractions to total tissue volume (BV/TV, %) from micro-CT scans. The pull-out mechanism of adding the β-TCP phase into the brushite system supports the decomposition and new bone formation in vivo compared with BR60. BV/TV values at the interface were (5.68 ± 1.05), (5.93 ± 1.13), and (7.96 ± 1.14) % for BR60, BR4P2, and BR4P2C, respectively, as summarized in Figure 6d. These values are expressed as the standard error. Bone formation at the interface is of our interest owing to the often large interfacial gap between the implant and the host bone. In addition, the greatest value was discovered for the BR4P2C implanted sample; it was evident that the BR4P2C system possessed an outstanding capacity for bone regeneration.

Histological examination with H&E and MT stains (Figures 7 and 8) assessed bone regrowth in all groups. At 1 month, the

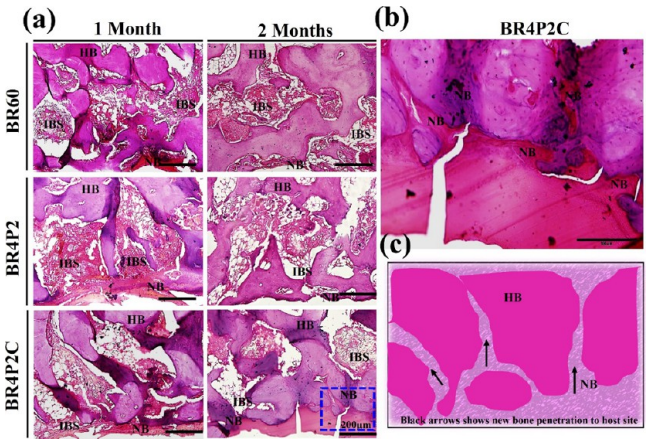

Figure 7. (a) H&E-stained images showing the extent of bone formations in the implanted zone after 1 and 2 months of implantation. (b) Enlarged image of blue dotted area for 2 months of BR4P2C. (c) Schematic illustration of new bone penetration into the host bone. Scale bar is 200 μm; HB: host bone; NB: new bone; IBS: injected bone substitute.

implant surface was surrounded by macrophages, neutrophils, and fibrous structures due to the acidic conditions created by brushite cement. Although these cell types were present, all implanted samples could still build a strong bond between the implant and the host bone. The tissue around the injection site responded generally to the foreign substances, suggesting that the initial acidic conditions had no effect. The data show that BR4P2C integrates well with the host bone and promotes better bone repair. Bone development at the defect margin was observed in all tested samples after 1 month. Dissolution products from BR4P2 and BR4P2C at the interface created space for bone osteoblast and osteoclast cells, accelerating the natural resorption of the implant. The histological findings showed that the β-TCP microspheres were topped with neo bone and degraded over time. The surface shape and porous structure of BR4P2C ensured in vitro cell adhesion and growth since bone graft features such as high porosity, appropriate

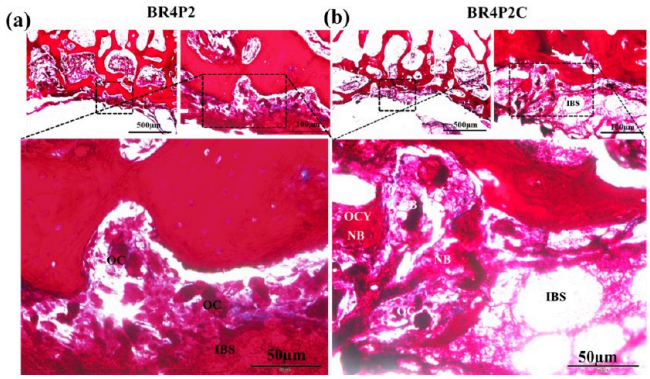

Figure 8. MT-stained images showing the extent of bone formations in the (a) BR4P2 and (b) BR4P2C implanted zones after 2 months of implantation. NB: new bone; IBS: injected bone substitute; OB: osteoblast; OC: osteoclast; and OCY: osteocytes.

pore diameters, and surface roughness allow nutrition and oxygen passage for cell attachment and growth. Bone cell recruitment is influenced by brushite and curcumin dissolution products exposed to the the physiological environment. Alternately, deterioration of the implant material was observed after 2 months, although fresh bone growth occurred along the margins of the defects, as summarized in Figure 7. Figure 8 shows the MT images of BR4P2 and BR4P2C after 2 months of implantation. In the case of BR4P2, there was not much new bone formation, but osteoclast and osteoblast activity could be easily monitored. BR4P2C interestingly showed new bone formation at the interface as well as penetrated into the host bone. Osteoclast activity can be easily monitored based on the presence of osteocytes in the new bone region. Osteoblast cells acted well to support new bone formation at the interface. The intact bone formation could be observed at the interface zone. In summary, this method may be helpful for drug loading and may also speed healing through mechanisms including regulated breakdown and function-specific cellular growth.

Scheme 2 illustrates the reaction mechanism explaining bone regeneration for each set of tested samples. The detailed scheme shows how brushite, sintered β-TCP microspheres, and curcumin affected in vivo bone remodeling and preserved the in vivo osteoclast/osteoblast cell balance. To a large extent, curcumin was identified to be responsible for the upregulation of ALP, OPN, and Col I. Furthermore, it acts as an anti-inflammatory candidate, reducing the inflammation risk in vivo.

4. CONCLUSIONS

In this study, we successfully developed and characterized a novel brushite-based IBS by incorporating curcumin. The BRPC composite demonstrated strong osteogenic properties, as evidenced by the activation of the ALP/OCN signaling pathway, which confirmed its ability to promote the differentiation of preosteoblasts into osteoblasts in vitro. These findings highlight the potential of the composite for enhancing bone regeneration at the cellular level.

In vivo experiments conducted using a rabbit animal model further validated the efficacy of the BR4P2C IBS. Compared to other implanted bone substitutes, the BR4P2C composite showed superior performance, evidenced by its ability to initiate early degradation and promote the formation of new bone tissue at the implantation site. The composite not only facilitated osteogenesis but also demonstrated effective

https://doi.org/10.1021/acsomega.4c10336
ACS Omega 2025, 10, 14961−14971

Scheme 2. Schematic Illustration of Bone Regeneration of Implanted Materials at the Implant Site

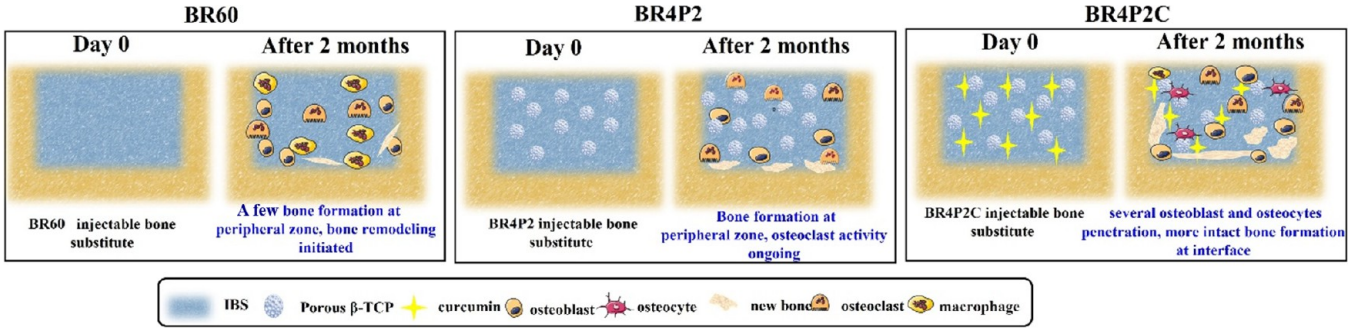

integration with the surrounding bone tissue, ensuring stable bonding at the bone interface.

The favorable osteogenic effects, combined with its biocompatibility and degradation profile, suggest that the BR4P2C macromolecule is a promising candidate for advancing the therapeutic application of active IBS. This innovative material could significantly improve clinical outcomes in bone repair and regeneration, offering a reliable solution for challenging bone defects and fractures. Moreover, the incorporation of curcumin provides additional bioactive benefits, potentially enhancing the healing process and overall therapeutic effectiveness. Overall, the BR4P2C IBS represents a step forward in the development of advanced materials for bone tissue engineering, with substantial potential for clinical translation.

■ ASSOCIATED CONTENT

Supporting Information

The Supporting Information is available free of charge at https://pubs.acs.org/doi/10.1021/acsomega.4c10336.

β-TCP porous microsphere preparation and SEM images of porous *β*-TCP microspheres (PDF)

■ AUTHOR INFORMATION

Corresponding Author

Byong-Taek Lee − *Institute of Tissue Regeneration and Department of Regenerative Medicine, College of Medicine, Soonchunhyang University, Cheonan 31204, South Korea;* orcid.org/0000-0001-9072-0033; Email: lbt@sch.ac.kr

Authors

Garima Tripathi − *Institute of Tissue Regeneration, Soonchunhyang University, Cheonan 31204, South Korea*

Myeongki Park − *Department of Regenerative Medicine, College of Medicine, Soonchunhyang University, Cheonan 31204, South Korea*

Seong-su Park − *Department of Regenerative Medicine, College of Medicine, Soonchunhyang University, Cheonan 31204, South Korea*

Hai-Doo Kim − *Institute of Tissue Regeneration, Soonchunhyang University, Cheonan 31204, South Korea*

Byoung-Ryol Lee − *ZNEXBIO, Asan 31538, South Korea*

Complete contact information is available at: https://pubs.acs.org/10.1021/acsomega.4c10336

Notes

The authors declare no competing financial interest.

G.T.: Conceptualization, methodology, formal analysis, data curation, investigation, and writing, review, and editing of the manuscript. M.P.: Formal analysis and data curation. S.-S.P.: Formal analysis and data curation. H.-D.K.: Provided porous *β*-TCP. B.-R.L.: Funding acquisition. B.-T.L.: Project administration, conceptualization, funding acquisition, and review and editing of the manuscript.

■ ACKNOWLEDGMENTS

This work was made possible by a grant (2015R1A6A1A03032522) from the Ministry of Education Basic Science Research Program administered by the National Research Foundation (NRF) Korea and Technology Development Program (Project No. RS-2023-00281111) funded by the Ministry of SMEs and Startups. It was also partially financed by Soonchunhyang University in South Korea.

■ REFERENCES

(1) Richter, R. F.; Vater, C.; Korn, M.; Ahlfeld, T.; Rauner, M.; Pradel, W.; Stadlinger, B.; Gelinsky, M.; Lode, A.; Korn, P. Treatment of critical bone defects using calcium phosphate cement and mesoporous bioactive glass providing spatiotemporal drug delivery. *Bioactive Materials* **2023**, *28*, 402−419.

(2) Wang, X. H.; Jia, S. J.; Hao, D. J. Advances in the modification of injectable calcium-phosphate-based bone cements for clinical application. *Chin Med. J. (Engl)* **2020**, *133*, 2610−2612.

(3) Dorozhkin, S. V. Calcium Orthophosphate Cements and Concretes. *Materials (Basel).* **2009**, *19*, 221−291.

(4) Cai, Z.; Jiang, H.; Lin, T.; Wang, C.; Ma, J.; Gao, R.; Jiang, Y.; Zhou, X. Microspheres in bone regeneration: Fabrication, properties and applications. *Materials Today Advances* **2022**, *16*, No. 100315.

(5) Ben, Y.; Zhang, L.; Wei, S.; Zhou, T.; Li, Z.; Yang, H.; Wang, Y.; Selim, F. A.; Wong, C.; Chen, H. PVB modified spherical granules of *β*-TCP by spray drying for 3D ceramic printing. *J. Alloys Compd.* **2017**, *721*, 312−319.

(6) Oliveira, R. L. M. S.; Motisuke, M. Using round *α*-TCP granules for improving CPC injectability. *Mater. Res. Express* **2019**, *6*, 125407.

(7) Stanić, Z. Curcumin, a Compound from Natural Sources, a True Scientific Challenge - A Review. *Plant Foods Hum Nutr* **2017**, *72*, 1−12.

(8) Aggarwal, B. B.; Kumar, A.; Bharti, A. C. Anticancer potential of curcumin: preclinical and clinical studies. *Anticancer Res.* **2003**, *23*, 363−398.

(9) Nakmareong, S.; Kukongviriyapan, U.; Pakdeechote, P.; Donpunha, W.; Kukongviriyapan, V.; Kongyingyoes, B.; Sompamit, K.; Phisalaphong, C. Antioxidant and vascular protective effects of curcumin and tetrahydrocurcumin in rats with L-NAME-induced hypertension. *Naunyn Schmiedebergs Arch Pharmacol* **2011**, *383*, 519−529.

(10) Kuo, M. L.; Huang, T. S.; Lin, J. K. Curcumin: an antioxidant and anti-tumor promoter, induces apoptosis in human leukemia cells. *Biochim. Biophys. Acta* **1996**, *1317*, 95−100.

(11) Hariri, M.; Haghighatdoost, F. Effect of Curcumin on Anthropometric Measures: A Systematic Review on Randomized Clinical Trials. *J. Am. Coll Nutr* **2018**, *37*, 215−222.
(12) Xu, C.; Wang, M.; Guo, W.; Sun, W.; Liu, Y. Curcumin in Osteosarcoma Therapy: Combining with Immunotherapy, Chemotherapeutics, Bone Tissue Engineering Materials and Potential Synergism With Photodynamic Therapy. *Frontiers in Oncology* **2021**, *11*, No. 672490.
(13) Al-Bishari, A. M.; Al-Shaaobi, B. A.; Al-Bishari, A. A.; Al-Baadani, M. A.; Yu, L.; Shen, J.; Cai, L.; Shen, Y.; Deng, Z.; Gao, P. Vitamin D and curcumin-loaded PCL nanofibrous for engineering osteogenesis and immunomodulatory scaffold. *Front Bioeng Biotechnol* **2022**, *10*, No. 975431.
(14) Kang, H.; Park, S.; Tripathi, G.; Lee, B. Injectable demineralized bone matrix particles and their hydrogel bone grafts loaded with β-tricalcium phosphate powder and granules: A comparative study. *Materials Today Bio* **2022**, *16*, No. 100422.
(15) Bose, S.; Sarkar, N.; Banerjee, D. Effects of PCL, PEG and PLGA polymers on curcumin release from calcium phosphate matrix for in vitro and in vivo bone regeneration. *Materials Today Chemistry* **2018**, *8*, 110−120.
(16) Wu, F.; Zhao, H.; Shi, J.; Long, L.; Yang, Z.; Jin, H.; Hou, X. Preparation and evaluation of an injectable curcumin loaded chitosan/hydroxyapatite cement. *J. Biomater Appl.* **2021**, *35*, 1372−1379.
(17) Sarkar, N.; Bose, S. Liposome-Encapsulated Curcumin-Loaded 3D Printed Scaffold for Bone Tissue Engineering. *ACS Appl. Mater. Interfaces* **2019**, *11*, 17184−17192.
(18) Tripathi, G.; Park, M.; Hossain, M.; Im, S. B.; Lee, B. T. Fabrication and characterization of cellulose nano crystal and soya modified injectable brushite bone cement for enhanced bone regeneration. *Inter. J. of Bio. Macromolecules* **2022**, *221*, 1536−1544.
(19) Li, X.; Chen, Y.; Mao, Y.; et al. Curcumin protects osteoblasts from oxidative stress-induced dysfunction via GSK3β-Nrf2 signaling pathway. *Frontiers in Bioengineering and Biotechnology* **2020**, *8*, 625−630.
(20) Chen, S.; Liang, H.; Ji, Y.; et al. Curcumin modulates the crosstalk between macrophages and bone mesenchymal stem cells to ameliorate osteogenesis. *Frontiers in Cell and Developmental Biology* **2021**, *9*, No. 634650.
(21) Dalal, P. V.; Saraf, K. B. Growth and study of barium oxalate single crystals in agar gel. *Bulletin of Materials Science* **2006**, *29*, 421−425.
(22) Rajendran, K.; Dale, C. Keefe Growth and characterization of calcium hydrogen phosphate dihydrate crystals from single diffusion gel technique. *Cryst. Res. Technol.* **2020**, *45*, 939−945.
(23) Wang, Z.; Nogueira, L. P.; Haugen, H. J.; Van Der Geest, I. C. M.; de Almeida Rodrigues, P. C.; Janssen, D.; Bitter, T.; Jeroen, C. G.; van den Beucken, J. J. P.; Leeuwenburgh, S. Dual-functional porous and cisplatin-loaded polymethylmethacrylate cement for reconstruction of load-bearing bone defect kills bone tumor cells. *Bioactive Mater.* **2022**, *15*, 120−130.
(24) Boşca, A. B.; Ilea, A.; Soriţău, O.; Tatomir, C.; Miklášová, N.; Pârvu, A. E.; Mihu, C. M.; Melincovici, C. S.; Fischer-Fodor, E. Modulatory effect of curcumin analogs on the activation of metalloproteinases in human periodontal stem cells. *Eur. J. Oral. Sci.* **2019**, *127*, 304−312.
(25) Foster, B. L.; Ao, M.; Salmon, C. R.; Chavez, M. B.; Kolli, T. N.; Tran, A. B.; Chu, E. Y.; Kantovitz, K. R.; Yadav, M.; Narisawa, S. Osteopontin regulates dentin and alveolar bone development and mineralization. *Bone* **2018**, *107*, 196−207.

https://doi.org/10.1021/acsomega.4c10336
ACS Omega 2025, 10, 14961−14971